Ultrasonics Sonochemistry 20 (2013) 799–804

Contents lists available at SciVerse ScienceDirect

Ultrasonics Sonochemistry

journal homepage: www.elsevier.com/locate/ultson

Short Communication

Morphological modifications and surface amorphization in ZnO sonochemically treated nanoparticles

Larisa B. Arruda [a], Marcelo O. Orlandi [b], Paulo Noronha Lisboa-Filho [c,*]

[a] POSMAT – Programa de Pós-Graduação em Ciência e Tecnologia de Materiais UNESP, Bauru, Brazil
[b] UNESP Univ Estadual Paulista, Instituto de Química, Departamento de Físico-Química, Araraquara, Brazil
[c] UNESP Univ Estadual Paulista, Faculdade de Ciências, Departamento de Física, Bauru, Brazil

ARTICLE INFO

Article history:
Received 9 April 2012
Received in revised form 24 November 2012
Accepted 24 November 2012
Available online 7 December 2012

Keywords:
Semiconductors
Nanoparticles
ZnO
Amorphous
Electron microscopy

ABSTRACT

Application of nanoscale materials in photovoltaic and photocatalysis devices and photosensors are dramatically affected by surface morphology of nanoparticles, which plays a fundamental role in the understanding of the physical and chemical properties of nanoscale materials. Zinc oxide nanoparticles with an average size of 20 nm were obtained by the use of a sonochemical technique. X-ray diffraction (XRD) associated to Rietveld refinements and transmission electron microscopy (TEM) were used to study structural and morphological characteristics of the samples. An amorphous shell approximately 10 nm thick was observed in the ultrasonically treated sample, and a large reduction in particle size and changes in the lattice parameters were also observed.

1. Introduction

Materials at the nanoscale usually present physical properties more diverse than their bulk counterparts, mainly due to electronic properties, where higher electronic density of states are present without continuous bands [1]. In addition, due to their high surface-to-volume ratio and possible surface defects, nanoparticles offer a unique opportunity for applications in nanoscale electronics.

Zinc oxide is a well-known direct wide band gap material (3.37 eV) with large exciton binding energy (60 meV). The controlled obtaining of stable ZnO nanostructures with different shapes and morphologies is a big challenge for science and industry as they are used as gas sensors [2], piezoelectric transducers, varistors, transparent conducting films [3], short wavelength light emitting devices, and electron field emitters [4], among many other applications. Particular to ZnO nanoparticles, activity and phase stability is directly affected by ZnO morphology. Considering photocatalytic activity, surface particles play a crucial role [5].

There are several synthesis routes to obtain nanoscale ZnO. Among the chemical routes, there are the sol–gel method [6] and hydrothermal [7,8], while physical routes include the ball milling process, sputtering, and laser ablation [9–11]. More recently, a new method to obtain nanostructured materials was presented, producing high-quality samples [12]. In this method, the main phenomenon is the acoustic cavitation, which leads to the formation, growth, and collapse of bubbles in the liquid. The growth of cavitation bubbles occurs due to the diffusion of solute vapor in the volume of these bubbles, which are generated through the vibration movement of the ultrasonic waves. After the growth process, which will depend on the liquid and the wave frequency, the bubbles reach the final stage, where they collapse, breaking the chemical bonds of the solute molecules [13]. Besides, collapsed bubbles can carry smaller particles, causing shocks among them, and possibly causing surface amorphization, which may result in their sintering. During this process, the extreme conditions generated at located points results in temperature around 5000 °C, pressures of 1000 atm, and heating and cooling rates of 10^{11} K/s [14].

The effects of cavitation collapse in surface morphology could be crudely subdivided into chemical effects and mechanical effects. Sonochemical surface modification is a well-known chemical effect and is often used for functionalization of surfaces. Otherwise, the mechanical effects of ultrasound exposure are better known as mechanochemistry [15].

In this context, better knowledge of nanoparticle morphology and surface structure of the synthesized specimens is crucial, not only to improve chemical effects, but also to determine mechanical and optical properties of sonochemically synthesized nanoparticles.

Zinc oxide is well known to have a large defect-related photoluminescence (PL) due to oxygen vacancies, zinc interstitials and zinc vacancies. Also, PL is directly related to morphological

* Corresponding author.
E-mail address: plisboa@fc.unesp.br (P.N. Lisboa-Filho).

1350-4177/$ - see front matter © 2012 Elsevier B.V. All rights reserved.
http://dx.doi.org/10.1016/j.ultsonch.2012.11.013

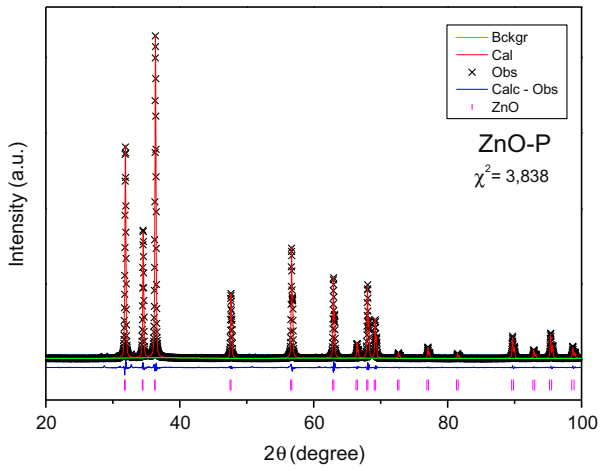

Fig. 1. Structural Rietveld refinement for the ZnO-P sample.

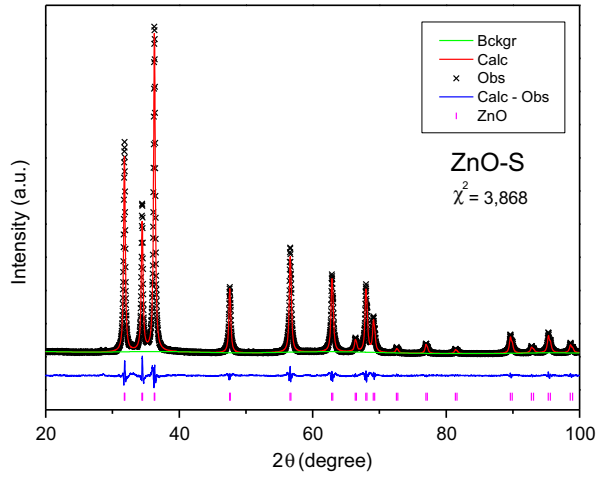

Fig. 2. Structural Rietveld refinement for the ZnO-S sonicated for 17 h.

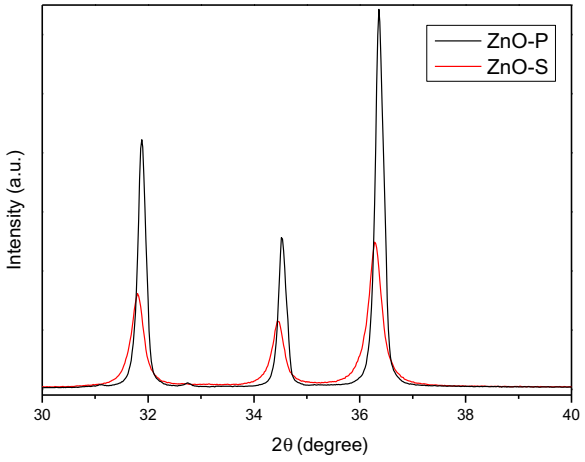

Fig. 3. Comparison of the main peaks of XDR of ZnO-P and ZnO-S samples.

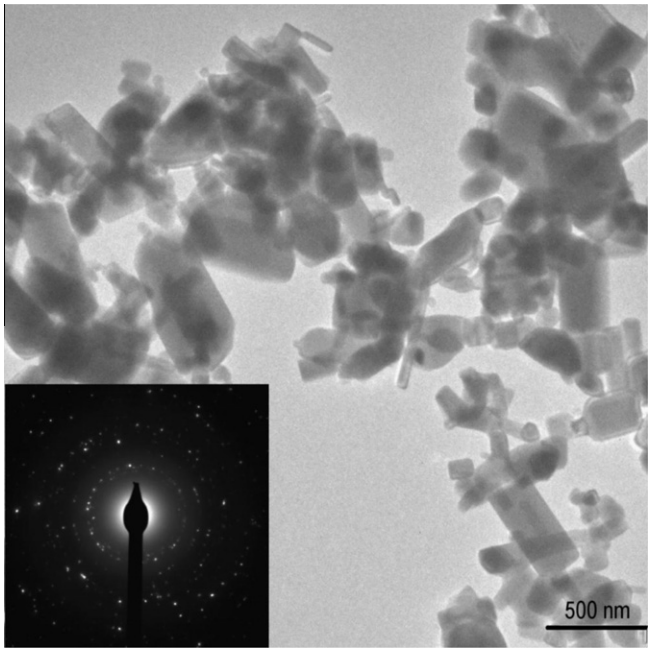

Fig. 4. TEM micrograph of the ZnO-P sample with monomodal distribution. In detail electron diffraction shows that this is a polycrystalline sample.

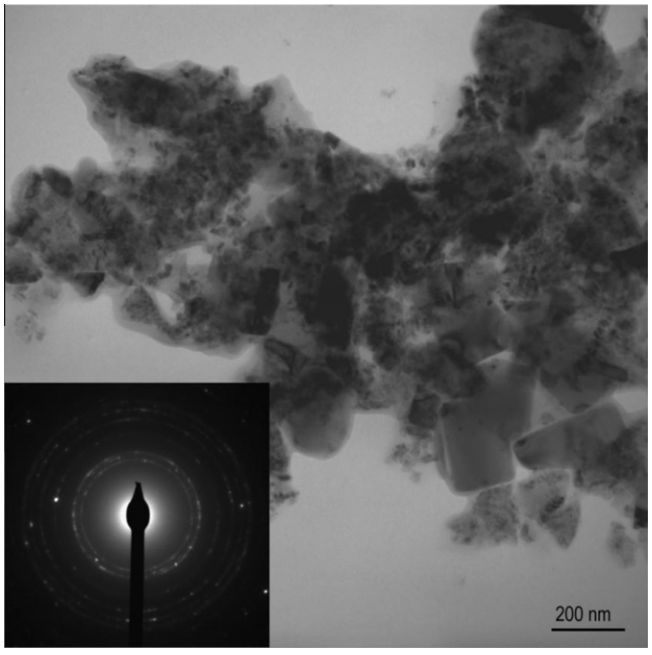

Fig. 5. TEM micrograph of the ZnO-S sample with bi-modal distribution. In detail electron diffraction.

characteristics of the nanoparticles [16]. Moreover, surface morphology is directly responsible for the charge carrier dynamics in nanoscale-based photovoltaic or photosensor devices [17].

This contribution reports a detailed investigation of nanoparticle morphology and surface amorphization in ZnO nanoparticles

Table 1
Lattice parameters obtained from structural refinement by Rietveld method for ZnO-P and ZnO-S.

Sample	Lattice parameters			Crystallite medium size (nm)		Chi^{2}	Rwp	R(F^{2})
	a (Å)	*c* (Å)	*V* (Å^3)	P//	P⊥			
ZnO-P	3.251856	5.209705	47.710	136.78	122.03	3.838	6.48	1.81
ZnO-S	3.249950	5.206927	47.628	31.25	32.37	3.868	7.05	1.47

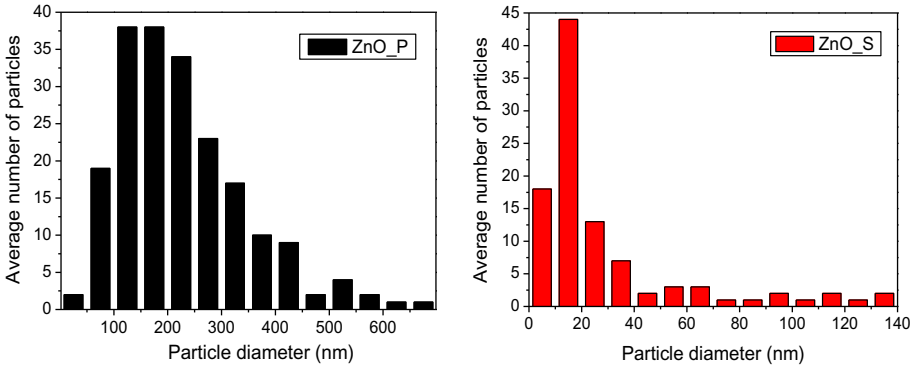

Fig. 6. Histograms of the distribution of number of particles as a function of particle diameter for the samples pure ZnO-P and sonicated ZnO-S.

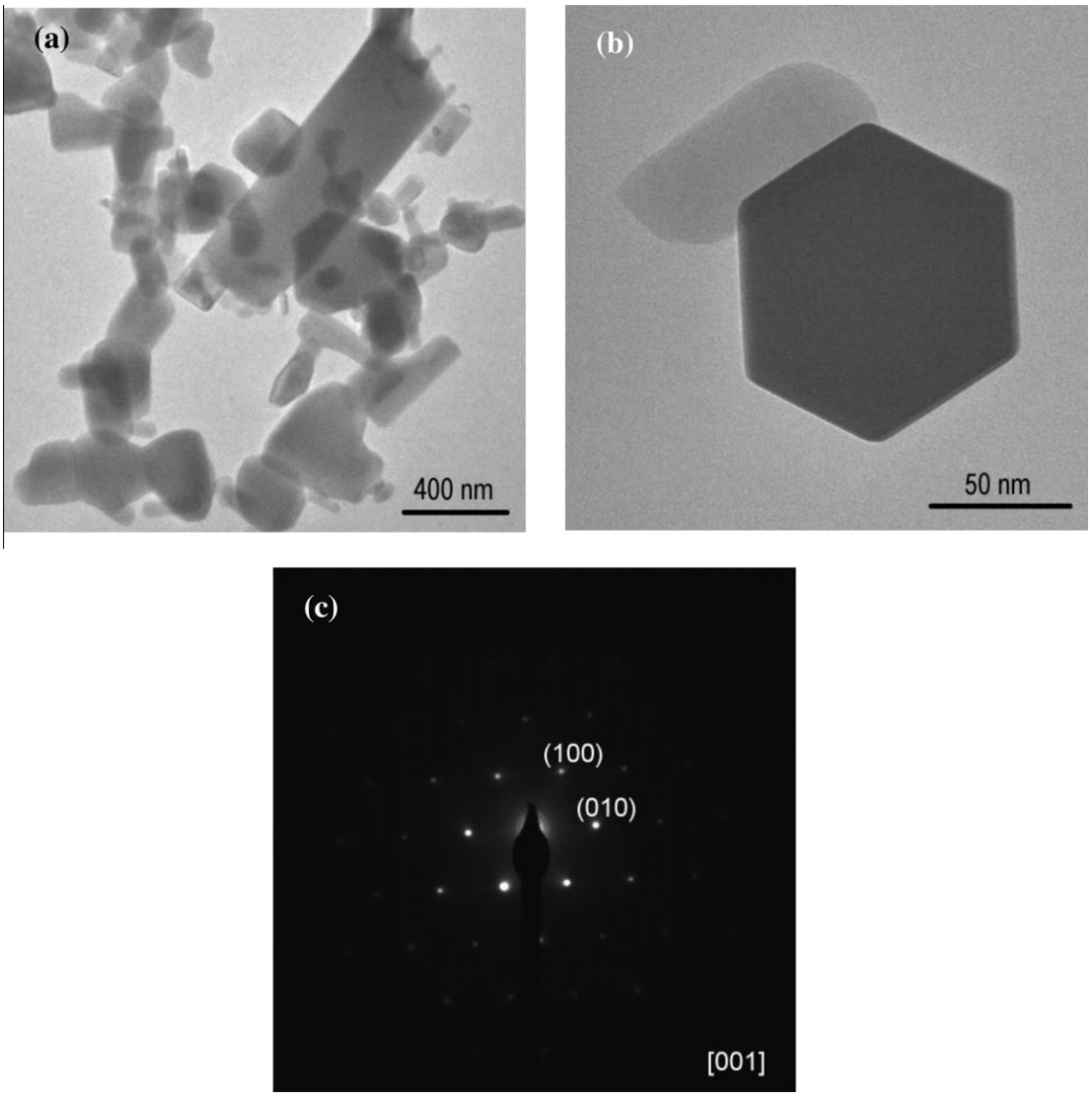

Fig. 7. TEM micrograph of the ZnO-P sample. (a) Particle size distribution is not homogeneous. (b) Single crystal ZnO. (c) Electron diffraction for single crystal of the image (b).

prepared by a sonochemical method. X-ray diffraction associated with Rietveld refinements, BET surface area measurements and transmission electron microscopy (TEM) were used as analytical tools to investigate structural and morphological properties of the samples.

2. Experimental details

Samples were obtained mixing 0.5 g of ZnO (Aldrich, 99,99%) in 100 ml isopropyl alcohol (C_3H_8O). The choice of isopropyl alcohol is due to its higher vapor pressure (4444 KPa – 20 °C), making

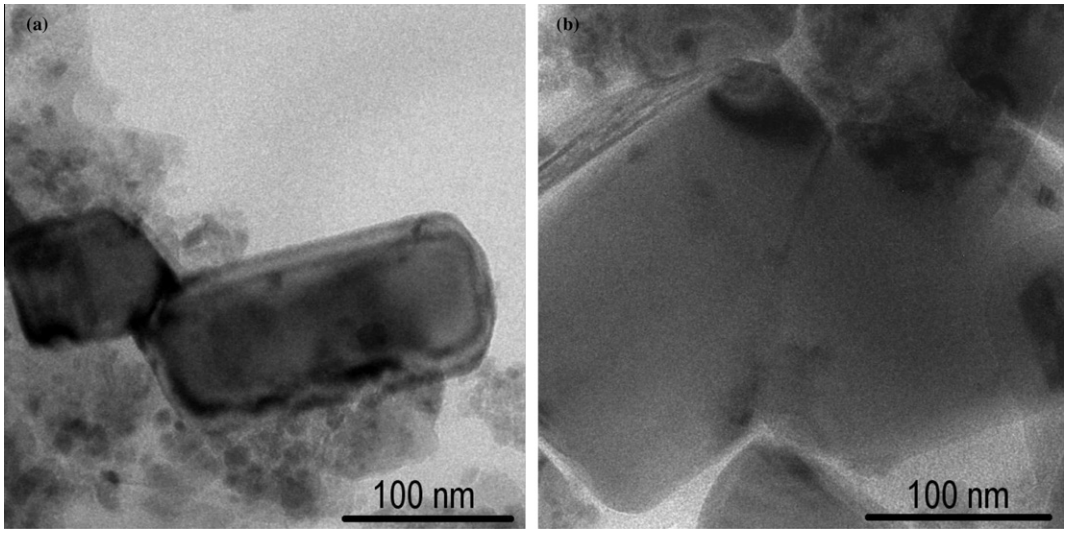

Fig. 8. (a) Selected TEM images of the ZnO-S sample showing a sintering process due to the sonication. (b) Magnified image confirming the coalescence of the sonicated particles.

the cavitation bubbles to have higher solute vapor, and thus accelerating the effect of acoustic cavitation.

One of the samples, labeled ZnO-P sample, is a pure commercial sample used as a reference. Another sample was submitted to ultrasonic processing in a Sonics brand model VCX-750, 750 W of power and frequency of 20 kHz for 17 h, with pulses of 5 min and variable amplitude fixed up to 90% from the nominal amplitude of the equipment (508 W/cm^2). In the synthesis camera, the conditions were atmospheric air, and the container with the samples and the ultrasonic tip were cooled with an ice bath. This sample was labeled ZnO-S and was subsequently dried in an oven at 80 °C, and no further thermal-annealing treatment was performed.

Crystallographic phases were traced in a conventional diffractometer Rigaku D/MAX 2100PC. Rietveld refinements were obtained by the use of GSAS software. The TEM images were obtained with Philips microscope model CM200. The specific surface areas of the samples were determined by the BET method with nitrogen adsorption-desorption isotherms at liquid nitrogen temperature (77 K) using a Micromeritics, model ASAP 2010 instrument.

3. Results and discussion

Structural refinements for samples ZnO-P and ZnO-S are shown in Figs. 1 and 2, respectively. Both samples can be indexed by the hexagonal phase of ZnO. It is possible to verify that sample P has a better fit graph than the sonicated sample, as it is possible to observe blue lines (Calc-Obs) in Figs. 1 and 2, which represents the difference between the theoretical diffractogram (Calc) based on the crystal structure of ZnO, and experimental diffractogram (Obs).

For the non-ultrasonically treated sample (ZnO-P), a high crystalline diffraction pattern was observed. Otherwise, the 17 h ultrasonically treated sample showed features specifically striking with broad peaks, indicating the occurrence of a crystallite size reduction and an amorphization process.

Fig. 3 shows two distinctive features of the ultrasonically treated sample that directly affect the Bragg peak. The decrease in intensity and the consequent increasing in the peak width are caused by a reduction in the crystallite size. Moreover, the position in the 2θ peak is associated with strain in the lattice caused by the sonochemical treatment [18].

The obtained Rietveld refinement results are summarized in Table 1. It was observed that after ultrasonic treatment, cell-lattice parameters a and c suffered a small decrease that reflected the decreasing in the unit cell volume. Initially, unit cell parameters had a volume of 47.710 Å^3, and after the sonication process, a volume of 47.628 Å^3 was detected. Such reduction in the unit cell volume reflects the stress in the crystal lattice generated by possible distortions caused by ultrasonic shock waves.

Another effect caused by the ultrasonic treatment is one decreasing in the crystallite size. For the ZnO-S samples this decrease was approximately 70% of the average crystallite size if compared to the initial values of ZnO-P samples.

As shown in Fig. 4, the ZnO-P sample consists of particles with a large size and form distribution. The electron diffraction pattern, shown in the detail in Fig. 4, can be indexed as ZnO and indicates a polycrystalline sample, as expected.

The effects of ultrasonic treatment in the morphology of particles can be observed in Fig. 5. This image shows particle fragmentation due to the 17 h of ultrasound exposure, producing a narrow size distribution in this sample different from the sample ZnO-P. As it is possible to observe in the histograms in Fig. 6, each histogram was plotted considering diameters of 200 nm (two by particle). Diffraction pattern confirms this material is pure ZnO after sonication, and the closed rings are a result of smaller size, and therefore, better random distribution of particles.

Fig. 7a shows a representative feature of size distribution of particles for ZnO-P, with average sizes close to 200 nm. However, smaller spherical particles with a diameter up to 70 nm can also be detected. A closer characterization of particles indicated which one is a single crystal of ZnO, and Fig. 7b–c shows a ZnO hexagon and its respective diffraction pattern, indicating that this crystal grows in the (0001) direction. These particles decrease significantly when sonicated, acquiring an average size of 20 nm, while they keep a single crystal characteristic.

Fig. 8a also shows that ultrasound may promote the sintering of particles. In our samples, this effect was not dominant, however some samples treated by long ultrasonic exposure showed such a characteristic. This sintering process is not the result of the high heat because these occur at located points, but is due to mechanical agitation that occurs in the middle caused by sound waves, which in turn lead the particles to collide with each other, and in some cases, cause coalescence of these. A detailed view of the sintering process can also be seen in Fig. 8b.

Furthermore, the sonication process also induces the occurrence of an amorphous cap layer in some particles, as can be seen

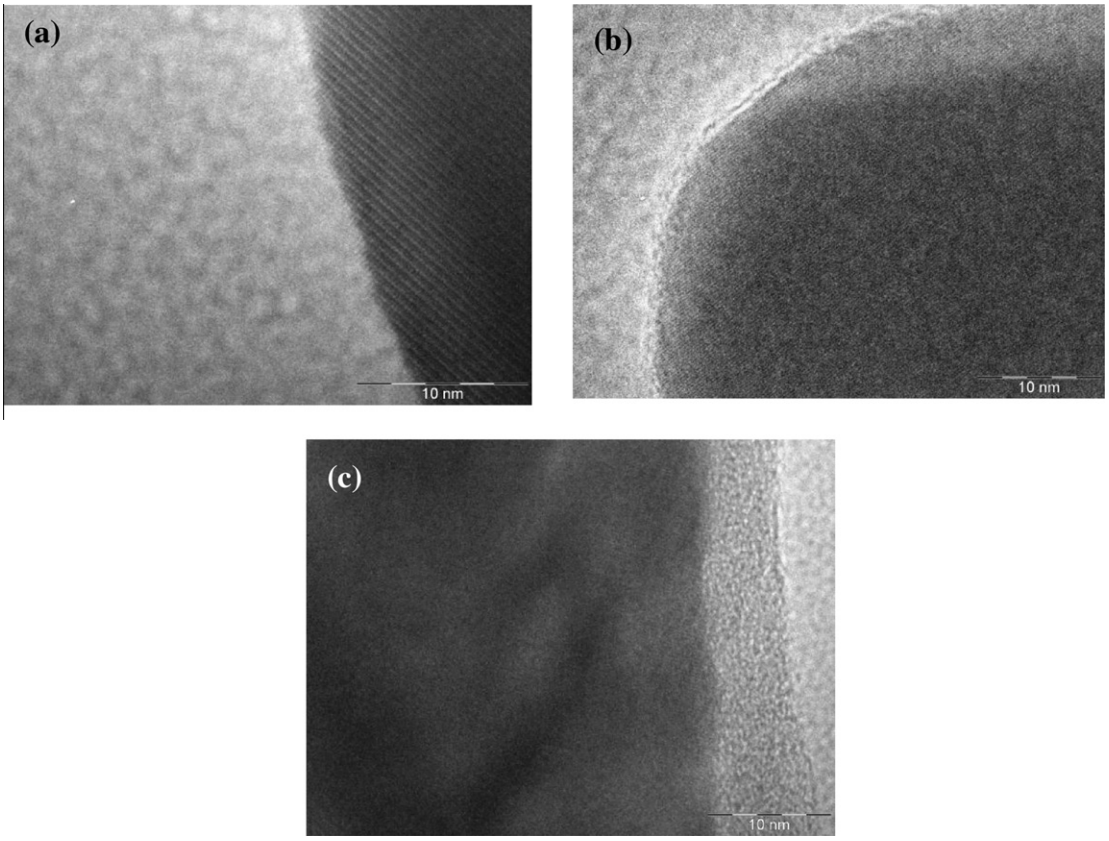

Fig. 9. TEM micrograph showing the evolution of the formation of surface amorphization for: (a) Sample pure ZnO-P. (b) 10 h ultrasonic exposure. (c) 17 h ultrasonic exposure.

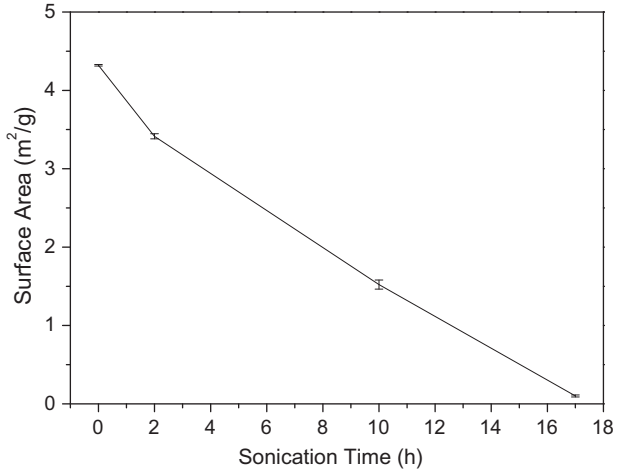

Fig. 10. BET surface area as a function of the ultrasonic exposure time.

in Fig. 9. Considering the non-treated sample ZnO-P, Fig. 9a shows no amorphous cap layer. However, an amorphization process is observed as sonication time increases. In Fig. 9b, a layer of 3 nm is observed for a sample treated for 10 h and a much more evident amorphous cap layer of 10 nm is detected for a sample sonicated for 17 h, indicating that the sonication process can induce amorphization in ZnO particles.

The specific surface areas of samples were determined by the BET method with nitrogen adsorption – desorption isotherms at liquid nitrogen temperature (77 K). According to the BET measurements, shown in Fig. 10, it is possible to observe that surface area decreases as the time of ultrasonic exposure increases. This result is characteristic for samples prepared under sonochemical conductions [19] considering that it also induces particles to form agglomerates [20], as seen in Fig. 5.

In our study of the microstructural effects of ultrasonic exposure, we may conclude that the sonochemical technique promotes three characteristic effects. The first one is the reduction of lattice parameters associated with a decrease in the average particle size. Moreover, a second effect is particle fragmentation due to collisions between particles during the acoustic cavitation process. Finally, surface amorphization may occur in some particles, provoking the occurrence of an amorphous surface layer.

Acknowledgments

The authors wish to thank Brazilian agencies Fundação de Amparo à Pesquisa do Estado de São Paulo - FAPESP (research project 2009/14628-6) and CNPq (304810/2010-0) for financial support.

References

[1] A. Janotti, C.G. Van de Walle, Fundamentals of zinc oxide as a semiconductor, Reports on Progress in Physics 72 (2009) 1–29.
[2] J. Liu, Z. Guo, F. Meng, T. Luo, M. Li, J. Liu, Novel porous single-crystalline ZnO nanosheets fabricated by annealing $ZnS(en)_{0.5}$ (en = ethylenediamine) precursor. Application in a gas sensor for indoor air contaminant detection, Nanotechnology 20 (2009) 1–8.
[3] D.C. Look, Recent advances in ZnO materials and devices, Materials Science and Engineering B 80 (2001) 383–387.
[4] Y.J. Zeng, S.S. Lin, A. Volodin, Y.F. Lu, Z.Z. Ye, C. Van Haesendonck, Zero-dimensional field emitter based on ZnO quantum dots, Applied Physics Letters 97 (2010) 1431021–1431023.

[5] M.Y. Guo, A.M. Ching Ng, F. Liu, A.B. Djurisic, W.K. Chan, H. Su, K.S. Wong, Effect of native defects on photocatalytic properties of ZnO, The Journal of Physical Chemistry C 115 (2011) 11095–11101.
[6] A. Azam, F. Ahmed, N. Arshi, M. Chaman, A.H. Naqvi, Formation and characterization of ZnO nanopowder synthesized by sol–gel method, Journal of Alloys and Compounds 496 (2010) 399–402.
[7] L. Yu, F. Qu, X. Wu, Facile hydrothermal synthesis of novel ZnO nanocubes, Journal of Alloys and Compounds 504 (2010) L1–L4.
[8] S. Baruah, J. Dutta, Hydrothermal growth of ZnO nanostructures, Science and Technology of Advanced Materials 10 (2009) 1–18.
[9] Y.W. Lao, S.T. Kuo, W.H. Tuan, Influence of ball milling on the sintering behaviour of ZnO powder, Ceramics International 35 (2009) 1317–1320.
[10] Y. Bouznit, Y. Beggah, K. Djessas, RF magnetron sputtering of ZnO and Al-doped ZnO films from ceramic and nanopowder targets: a comparative study, Journal of Sol-Gel Science and Technology 61 (2012) 449–454.
[11] X. Hu, H. Gong, H. Xu, H. Wei, B. Cao, G. Liu, H. Zeng, W. Cai, Influences of target and liquid media on morphologies and optical properties of ZnO nanoparticles prepared by laser ablation in solution, Journal of the American Ceramic Society 94 (2011) 4305–4309.
[12] J.H. Bang, K.S. Suslick, Applications of ultrasound to the synthesis of nanostructured materials, Advanced Materials 22 (2010) 1039–1059.
[13] A. Gedanken, Using sonochemistry for the fabrication of nanomaterials, Ultrasonics Sonochemistry 11 (2004) 47–55.
[14] K.S. Suslick, M.M. Fang, T. Hyeon, M.M. Mdleleni, Applications of sonochemistry to materials synthesis, Sonochemistry and Sonoluminescence (1999) 291–320.
[15] T.J. Mason, A.J. Cobley, J.E. Graves, D. Morgan, New evidence for the inverse dependence of mechanical and chemical effects on the frequency of ultrasound, Ultrasonics Sonochemistry 18 (2011) 226–230.
[16] J.B. Cui, M.A. Thomas, Power dependent photoluminescence of ZnO, Journal of Applied Physics 106 (2009) 033518.
[17] M. Li, G. Xing, L.F.N. Ah Qune, G. Xing, T. Wu, C.H.A. Huan, X. Zhang, T.C. Sum, Tailoring the charge carrier dynamics in ZnO nanowires: the role of surface hole/electron traps, Physical Chemistry Chemical Physics 14 (2012) 3075–3082.
[18] A.K. Zak, W.H. Abd Majid, M.E. Abrishami, R. Yousefi, X-ray analysis of ZnO nanoparticles by Williamson-Hall and size-strain plot methods, Solid State Sciences 13 (2011) 251–256.
[19] N. Perkas, V.G. Pol, S.V. Pol, A. Gedanken, Gold-induced crystallization of SiO2 and TiO2 powders, Crystal Growth and Design 6 (2006) 293–296.
[20] S. Bhattacharyya, A. Gedanken, A template-free, sonochemical route to porous ZnO nano-disks, Microporous and Mesoporous Materials 110 (2008) 553–559.